

Uniformly rotating rings in general relativity

Thomas Fischer,¹ Stefan Horatschek^{1*} and Marcus Ansorg²

¹*Theoretisch-Physikalisches Institut, University of Jena, Max-Wien-Platz 1, 07743 Jena, Germany*

²*Max-Planck-Institut für Gravitationsphysik, Albert-Einstein-Institut, Am Mühlenberg 1, 14476 Golm, Germany*

Accepted 2005 September 19. Received 2005 September 2; in original form 2005 June 28

ABSTRACT

In this paper, we discuss general relativistic, self-gravitating and uniformly rotating perfect fluid bodies with a toroidal topology (without central object). For the equations of state describing the fluid matter, we consider polytropic as well as completely degenerate, perfect Fermi gas models. We find that the corresponding configurations possess similar properties to the homogeneous relativistic Dyson rings. On one hand, there exists no limit to the mass for a given maximal mass–density inside the body. On the other hand, each model permits a quasi-stationary transition to the extreme Kerr black hole.

Key words: gravitation – relativity – methods: numerical – stars: rotation.

1 INTRODUCTION

The first studies of uniformly rotating, axisymmetric and self-gravitating, toroidal perfect fluids in equilibrium date back to the 19th century, when Kowalewsky (1885), Poincaré (1885a,b,c) and Dyson (1892, 1893) considered thin homogeneous rings in Newtonian gravity. The analytical expansion found by Dyson is a fourth-order approximation of the solution to the corresponding free boundary value problem. Numerical investigations of these Dyson rings have been carried out by Wong (1974), Eriguchi & Sugimoto (1981) and Ansorg, Kleinwächter & Meinel (2003c). In their studies, Eriguchi and Sugimoto were able to confirm a conjecture by Bardeen (1971) about a continuous parameter transition of the Dyson ring sequence to the well-known Maclaurin spheroids. The analogues of these rings in Einsteinian gravity (the ‘relativistic Dyson rings’) were treated by Ansorg, Kleinwächter & Meinel (2003b).

Hachisu (1986) extensively studied both spheroidal and toroidal self-gravitating Newtonian fluid bodies (uniformly as well as differentially rotating) governed by different equations of state, among them polytropes (with polytropic index N varying from 0 to 4) and white dwarves (described by Chandrasekhar’s equation of a relativistic, completely degenerate, perfect Fermi gas). In particular, he presented the critical configurations which rotate at the mass-shedding limit and mark the endpoint of specific sequences. These investigations showed that, in contrast to the uniformly rotating homogeneous models, for all other equations of state considered, there exist disjoint Newtonian sequences of spheroidal and toroidal shape.

Proceeding to the relativistic realm, the uniformly rotating homogeneous bodies were also found to form disjoint classes.¹ The corresponding complete picture in Newtonian and Einsteinian

gravity is presented in Ansorg et al. (2003c) and Ansorg et al. (2004).

The aim of this paper is to extend Hachisu’s work to Einsteinian gravity. We study uniformly rotating polytropes (with polytropic indices N varying from 0 to 4) as well as neutron gas configurations with a toroidal shape. The neutron gas bodies are motivated by Chandrasekhar’s equation of state applied to a neutron star. Like Hachisu, we identify the mass-shedding configurations that bound our solution space.

Uniform rotation is widely used to describe rotating neutron stars. In particular, when restricting oneself to stationary solutions, it is all but necessary to consider this simple rotation law since any realistic matter would gradually smooth out any imposed differential rotation by means of some dissipative processes. In addition, note that through differential rotation a free function describing the angular velocity as it depends on the radius would enter into the game and a concise representation of some basic properties of the rings in question (as intended in our paper) would be difficult. Therefore, in this paper we focus our attention on uniform rotation.

As proved by Meinel (2004), only the extreme Kerr black hole can be the black hole limit of rotating perfect fluid bodies in equilibrium. In Ansorg et al. (2003b), a numerical example of such a transition to the extreme Kerr black hole was found for the relativistic Dyson rings. Here, we follow this line and find that such a transition is a general feature of ring configurations, i.e. it was found for all models studied.

Our numerical investigations are based on the highly accurate multidomain, pseudo-spectral method described in Ansorg, Kleinwächter & Meinel (2003a), which allows us to calculate even the limiting configurations very precisely.

In the units used, the speed of light as well as Newton’s constant of gravity is equal to 1.

2 METRIC TENSOR AND FIELD EQUATIONS

The line element for a stationary, axisymmetric space–time describing the gravitational field of a uniformly rotating perfect fluid body

*E-mail: sho@tpi.uni-jena.de

¹ They are only connected through specific bifurcation points of the Maclaurin sequence at which this sequence becomes secularly unstable with respect to axisymmetric perturbations and the post-Newtonian expansion fails.

can be written in Lewis–Papapetrou coordinates as follows:

$$ds^2 = e^{2\alpha}(d\varrho^2 + d\zeta^2) + W^2 e^{-2\nu}(d\varphi - \omega dt)^2 - e^{2\nu} dt^2. \quad (1)$$

We define these coordinates $(\varrho, \zeta, \varphi, t)$ uniquely by the requirement that all metric functions and their first derivatives be continuous everywhere, in particular at the fluid surface.

For a perfect fluid body rotating with the uniform angular velocity Ω , the following boundary condition at the fluid surface holds:

$$e^{2\nu} - W^2(\omega - \Omega)^2 e^{-2\nu} = \text{constant} = (1 + Z_0)^{-2}. \quad (2)$$

The constant Z_0 is the relative redshift measured at infinity of photons emitted from the body surface that do not carry angular momentum.²

Apart from the above boundary condition, regularity of the metric along the axis $\varrho = 0$ is required as well as reflectional symmetry with respect to the equatorial plane $\zeta = 0$. Taking the interior and exterior field equations, the transition conditions at the fluid surface, the above regularity requirements and the asymptotic behaviour at infinity, we obtain a complete free boundary problem to be solved. In particular, the unknown toroidal shape of the fluid body enters into this set of equations.

Note that for isolated general relativistic fluid bodies, the regularity condition at infinity is usually asymptotic flatness. However, the situation becomes more complex as the transition to the extreme Kerr black hole is considered (see Meinel 2002). In this limiting process, the ring shrinks down to the coordinate origin and the resulting exterior geometry is given by the extreme Kerr metric outside the horizon. On the contrary, a different non-asymptotically flat limit is encountered if the coordinates are rescaled in such a way that the extension of the ring remains finite. In this case, the behaviour of the gravitational potentials at infinity is determined by the ‘extreme Kerr throat geometry’ (Bardeen & Horowitz 1999).

3 THE EQUATIONS OF STATE

In order to consider a specific model of a rotating fluid configuration, it is essential to describe the matter inside the body by a characteristic equation of state. In this paper, we treat polytropic as well as completely degenerate, perfect Fermi gas models. The corresponding equations of state relate the mass–energy density μ and the pressure p , which enter the field equations through the energy–momentum tensor. It reads for a perfect fluid as follows:

$$T_{ik} = (\mu + p)u_i u_k + p g_{ik}, \quad (3)$$

with u^k being the four-velocity of the fluid elements.

For so-called isentropic models, especially in the zero temperature limit, a rest-mass density μ_B can be derived from

$$\frac{d\mu_B}{\mu_B} = \frac{d\mu}{\mu + p}. \quad (4)$$

The physical quantities μ , μ_B and p allow us to define a gravitational mass M as well as a rest mass M_0 , which we will use as characteristic parameters to describe a specific fluid configuration. Note that the constant of integration in equation (4) is fixed by the requirement that

$$\mu/\mu_B \rightarrow 1 \quad \text{as} \quad p \rightarrow 0. \quad (5)$$

² No angular momentum means $\eta_i p^i = 0$ (p^i : four-momentum of the photon, η^i : Killing vector corresponding to axisymmetry).

3.1 Polytropic models

The relativistic polytropic equation of state was given by Tooper (1965) as follows:

$$\mu = Np + (p/K)^{N/(N+1)}. \quad (6)$$

Here, N and K are the polytropic index and polytropic constant, respectively. In this paper, we vary N within the interval $[0, 4]$. For small values, the equation of state is called ‘stiff’, corresponding to a strong fall-off of the mass densities in the vicinity of the fluid surface. In particular, $N = 0$ describes the homogeneous model in which the mass densities (μ , μ_B) jump at the surface. On the other hand, we obtain a ‘soft’ equation of state for larger N , resulting in flat density profiles close to the fluid boundary.

Note that we may use the fundamental length $K^{N/2}$ in order to introduce dimensionless quantities,

$$\bar{M} = K^{-N/2} M, \quad \bar{\Omega} = K^{N/2} \Omega \quad (7)$$

(see Nozawa et al. 1998).

3.2 Chandrasekhar’s equation of state

Chandrasekhar’s equation of state describes a relativistic, completely degenerate, perfect Fermi gas (Oppenheimer & Volkov 1939). It is given implicitly by

$$\mu = K_C \left[(6x_F^3 + 3x_F) \sqrt{1 + x_F^2} - 3 \ln(x_F + \sqrt{1 + x_F^2}) \right], \quad (8)$$

$$p = K_C \left[(2x_F^3 - 3x_F) \sqrt{1 + x_F^2} + 3 \ln(x_F + \sqrt{1 + x_F^2}) \right]. \quad (9)$$

Here, the constant K_C ,

$$K_C = \frac{m^4(2s + 1)}{48\pi^2 \hbar^3}, \quad (10)$$

is derived from the mass m and the spin s of the fermions. Therefore, taking a neutron gas, the equation of state is completely fixed and does not contain any free parameters.

Note that $x_F = p_F/m$ is the dimensionless Fermi momentum of the gas. In the non-relativistic limit, $x_F \ll 1$, the equation of state approaches the polytropic equation of state with $N = 3/2$.

4 RESULTS

The studies of Hachisu (1986) provide an extensive overview of Newtonian ring configurations. For a number of equations of state, the characteristic features of the corresponding ring sequences are illustrated by means of specific parameter diagrams and tables. Moreover, the shapes of representative examples are displayed in cross-section.

With the transition to Einsteinian gravity, we have an additional relativistic parameter at our disposal which makes it difficult to give a similar detailed overview over the corresponding relativistic picture. We focus therefore our attention on the important question of parametric transitions of the relativistic objects to characteristic limiting configurations. As in Ansorg et al. (2003b), we identify the mass-shedding as well as the extreme Kerr black hole limit for each equation of state considered. For the polytropes with $N = 1$, we provide three parameter diagrams displaying the characteristic behaviour of representative physical quantities of the corresponding fluid bodies. Finally, we consider an exemplary sequence of Fermi gas fluid bodies with prescribed rest mass $M_0 = 24 M_\odot$ that terminates at the extreme Kerr black hole limit.

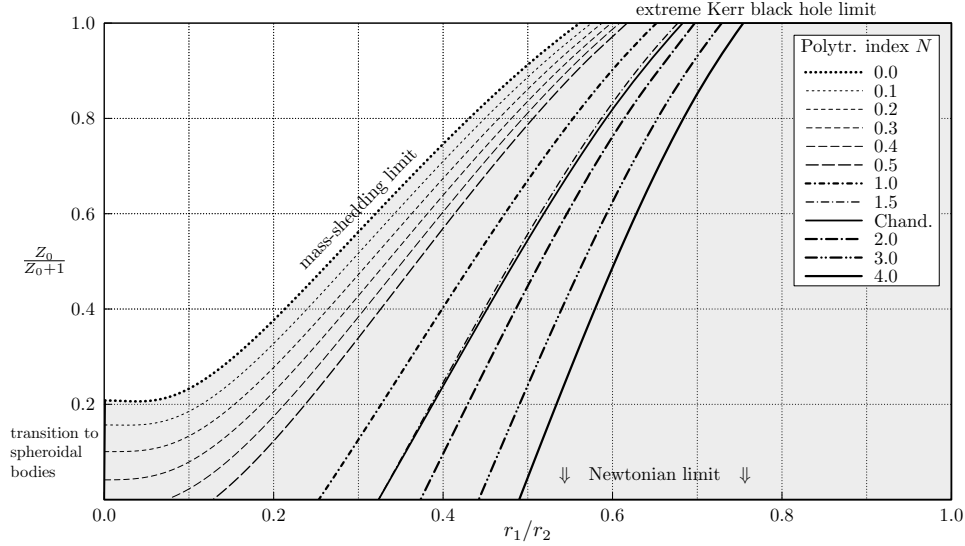


Figure 1. Parameter space of the rings considered in the $r_1/r_2 - Z_0/(Z_0 + 1)$ plane. Each parameter region corresponding to a particular equation of state is bounded from the left by a mass-shedding sequence. Note that the transition to the extreme Kerr black hole is exhibited for all matter models studied.

4.1 Parameter space of ring configurations

We may characterize each fluid body governed by a prescribed equation of state by two physical parameters. In Fig. 1, the relativistic quantity $Z_0/(1 + Z_0)$ is plotted against the ratio r_1/r_2 of the inner to outer (coordinate) radius of the rings. Note that $Z_0/(1 + Z_0)$ vanishes in the Newtonian limit and tends to unity in the extreme Kerr black hole limit.

The relativistic Dyson rings (described by the polytropic constant $N = 0$) possess parameter pairs that are located in the grey shaded area. Apart from the limit of infinitely thin rings ($r_1/r_2 \rightarrow 1$), this area is bounded by (i) the Dyson rings in Newtonian gravity, (ii) configurations at the transition to spheroidal topology, (iii) critical configurations that rotate at the mass-shedding limit³ and (iv) ultra-relativistic configurations at the transition to the extreme Kerr black hole (see Section 4.3).

If we increase the polytropic index N , we find that the mass-shedding sequence moves sideways. However, the corresponding areas are still bounded by the same types of limiting curves, among them the Newtonian sequences that were studied by Hachisu. Note that from a critical $N_{\text{crit}} \approx 0.35$ on, there is no continuous transition to spheroidal bodies, as exhibited by the fact that the mass-shedding sequence terminates at the Newtonian limit.

In Fig. 1, the parameter region with respect to Chandrasekhar's equation of state is also shown. Since these configurations have the same Newtonian limit as the polytropic rings with $N = 3/2$, the two corresponding mass-shedding sequences meet at the abscissa. We see that the overall deviation of these two curves remains small throughout the entire relativistic regime.

4.2 Polytropic rings with $N = 1$

As illustrated in Fig. 1, for the different matter models very similar results emerge. Let us, as an example, consider the class of rela-

tivistic polytropic rings with the polytropic index $N = 1$ in more detail.

Fig. 2 shows the quantities \bar{M} , M^2/J (J : angular momentum) and $\bar{\Omega}$ as functions of the radius ratio. The solid lines represent sequences of configurations with a constant prescribed value for the redshift ($Z_0 = e^{-V_0} - 1$). They terminate at the dashed line, which describes the mass-shedding sequence (cf. Fig. 1).

As with the relativistic Dyson rings, we find that the (dimensionless) mass \bar{M} grows to infinity in the thin ring limit. This result is also valid for the Dyson rings in Newtonian gravity, which can be proved analytically. In particular, for fixed V_0 we find that

$$\lim_{\sigma \rightarrow 0} [\bar{M} \sigma (-\ln \sigma)^{3/2}] = \sqrt{-\frac{32\pi}{125} V_0^3}, \quad (11)$$

where $\sigma = (r_2 - r_1)/(r_2 + r_1)$.

This subtle limit seems to possess unique features independent of the specific equation of state being considered. Note that we find the same typical behaviour of \bar{M} for both stiff and soft equations of state. We plan a more thorough investigation of this issue in a subsequent publication.

4.3 Quasi-stationary transition to the extreme Kerr black hole

As shown by Meinel (2004), the extreme Kerr solution is the only black hole limit of rotating perfect fluid bodies in equilibrium. It is characterized by an infinite redshift Z_0 . Indeed, if a sequence of fluid configurations possesses no upper bound for Z_0 , then this sequence necessarily admits the transition to the extreme Kerr solution (see Meinel 2005).

However, spheroidal configurations do not seem to exhibit this limit. In particular, for spherically symmetric static bodies $Z_0 < 2$ always holds, which is a consequence of the well-known Buchdahl limit. Numerical investigations have shown that $Z_0 < 7.378$ for the class of uniformly rotating homogeneous spheroidal bodies (Schöbel & Ansorg 2003). The corresponding critical configuration with this maximal redshift rotates at the mass-shedding limit and possesses infinite central pressure. Although the mass-shedding limit is the characteristic of maximal redshift configurations,

³ A mass-shedding limit is given if a fluid particle at the surface of the body moves with the same angular velocity as a test particle at that spatial point. The corresponding geometrical shape of the fluid body possesses a cusp there.

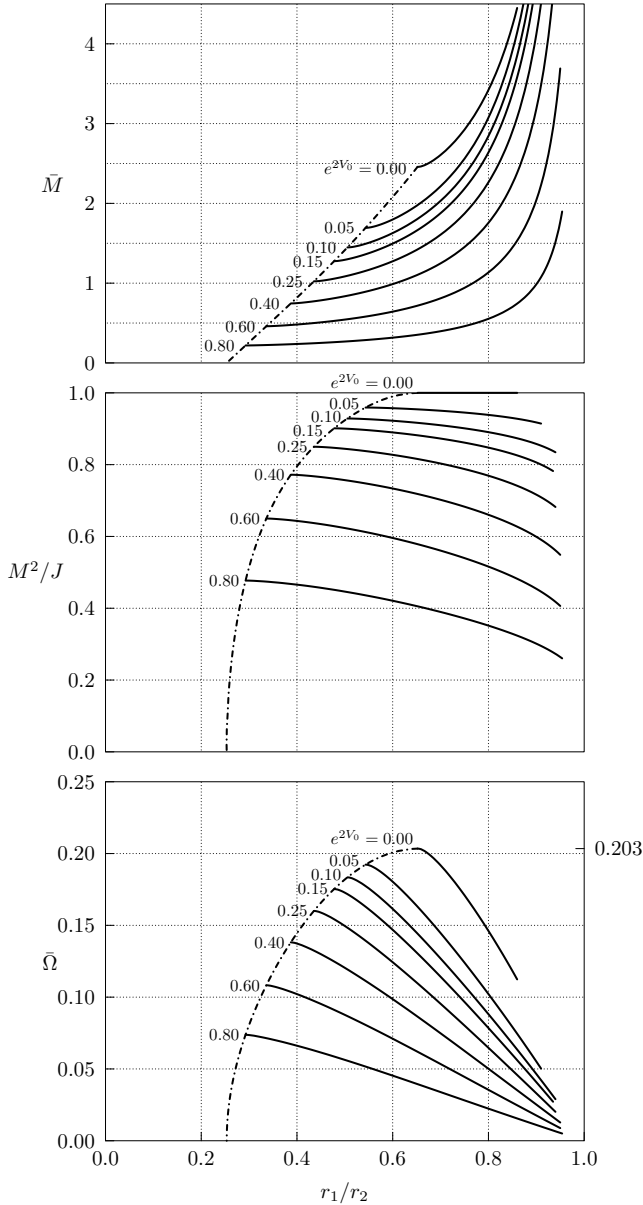


Figure 2. For polytropic rings with $N = 1$, the dimensionless gravitational mass \bar{M} , the (dimensionless) quantity M^2/J and the dimensionless angular velocity $\bar{\Omega}$ are plotted against the radius ratio r_1/r_2 for certain values of $e^{2V_0} = (1+Z_0)^{-2}$. The dashed lines describe the mass-shedding sequence.

infinite central pressure is not a typical feature (in particular, neither for Chandrasekhar’s nor for polytropic equations of state with $N > 0$ does maximal redshift coincide with infinite central pressure). It is interesting to note that the value of the maximal redshift decreases with increasing polytropic index N (therefore 7.378 is an upper bound). The maximal redshift for Chandrasekhar’s equation of state ($Z_0 \approx 0.217$) is quite close to the maximal redshift for the polytropic configurations with $N = 3/2$ ($Z_0 \approx 0.279$) (cf. the discussion at the end of Section 3.2).

In contrast, there is no upper bound for the redshift of discs of dust (Neugebauer & Meinel 1995) and fluid rings (Ansorg et al. 2003b). As mentioned at the end of Section 2, the corresponding limiting procedure can be performed in two different ways.

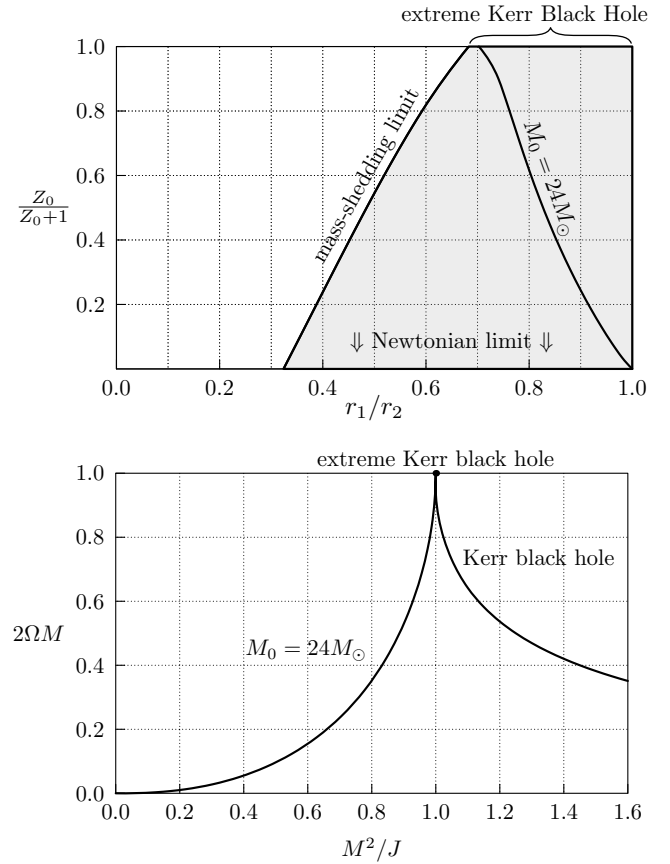


Figure 3. In the $r_1/r_2 - Z_0/(Z_0 + 1)$ plane, the mass-shedding sequence for rings governed by Chandrasekhar’s equation of state is shown (cf. Fig. 1). Moreover, the specific sequence of such rings with fixed $M_0 = 24 M_\odot$ is given. In the lower panel, this sequence is met by the sequence of Kerr black holes.

(i) If we consider some point in space outside the coordinate origin and hold the corresponding coordinates (ϱ, ζ) fixed during the limiting process, then we note that the equilibrium configuration shrinks down to the coordinate origin and the space–time assumes the exterior geometry of the extreme Kerr solution in Weyl coordinates.

(ii) If, on the contrary, we rescale the spatial coordinates such that (ϱ/r_2) and (ζ/r_2) remain finite [for more details see Meinel (2002), equations (47) and (54) therein], we obtain a solution of Einstein’s field equations that still describes an axisymmetric and stationary gravitational source in vacuum, but is no longer asymptotically flat. This interior, non-asymptotically flat solution is not unique. For each equation of state and a sufficiently large coordinate radius ratio (see Fig. 1), we get a distinct interior space–time. Moreover, in general a space–time of this kind does not necessarily contain a gravitational source of toroidal topology. As an important example of this, consider the infinite redshift limit of the analytically known solution corresponding to a rigidly rotating disc of dust (Neugebauer & Meinel 1995). In this limit, the gravitational source remains a disc whence the corresponding topology is different from a ring topology.

As pointed out in Meinel (2002), the above two limits of space–time geometries are disconnected from one another (the connection would be an ‘infinitely extended throat’). In this way, it is possible to obtain very different non-asymptotically flat interior limits and always the same exterior, extreme Kerr black hole limit.

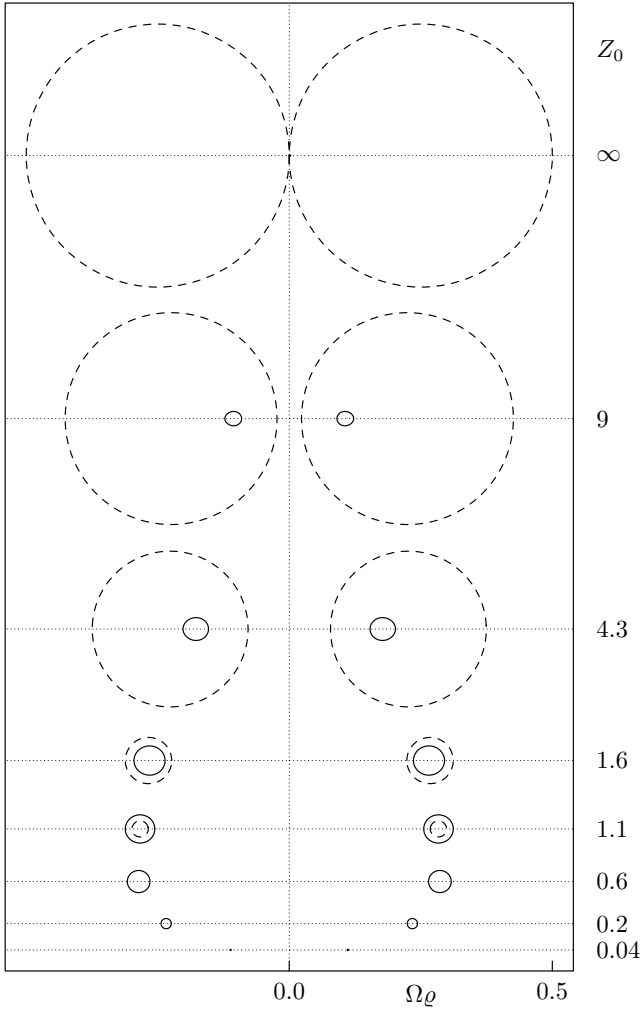


Figure 4. Meridional cross-sections (solid) and ergospheres (dashed) for the ring sequence $M = 24 M_{\odot}$ governed by Chandrasekhar's equation of state. The normalized ζ -coordinate, $\Omega\zeta$, is plotted against the normalized q -coordinate Ωq . In the limit $Z_0 \rightarrow 0$ as well as in the extreme Kerr black hole limit ($Z_0 \rightarrow \infty$), the ring shrinks down to the normalized coordinate origin.

In this section, we want to consider a specific sequence of configurations governed by Chandrasekhar's equation of state, which allows the parametric transition to the extreme Kerr black hole. Along this sequence, we hold the rest mass $M_0 = 24 M_{\odot}$ fixed.

From Fig. 3, we see that configurations with extremely small redshift Z_0 approach the limit of infinitely thin rings in the Newtonian limit. That underlines once more the sophisticated character of this limit: any sequence of configurations with bounded mass cannot

terminate at some $Z_0 > 0$ since all the points ($r_1/r_2 = 1$, $Z_0 > 0$) correspond to configurations with infinite masses (see Fig. 2). On the other hand, a sequence of finite mass configurations, $M_0 > 0$, cannot, of course, terminate in a Newtonian limit. The only remaining possibility for the curve in Fig. 3 is to move 'somewhere' between these limiting curves. Thus, the limit of infinitely thin rings is more complex than Figs 1 and 3 reveal.

As the redshift of the configurations in question increases, the ratio r_1/r_2 decreases to some minimal value $r_1/r_2 \approx 0.7$. At this point, the sequence approaches the extreme Kerr black hole limit in a way that is very similar to the example with $r_1/r_2 = 0.7$ discussed in Ansorg et al. (2003b). This is confirmed by Fig. 4 in which meridional cross-sections for selected configurations of this sequence are shown. Note that ergospheres appear above a certain redshift, which again is in agreement with the results obtained in Ansorg et al. (2003b).

ACKNOWLEDGMENTS

We would like to thank R. Meinel and D. Petroff for many valuable discussions and helpful advice. This research was funded in part by the Deutsche Forschungsgemeinschaft (SFB/TR 7-B1).

REFERENCES

- Ansorg M., Kleinwächter A., Meinel R., 2003a, *A&A*, 405, 711
 Ansorg M., Kleinwächter A., Meinel R., 2003b, *ApJ*, 582, L87
 Ansorg M., Kleinwächter A., Meinel R., 2003c, *MNRAS*, 339, 515
 Ansorg M., Fischer T., Kleinwächter A., Meinel R., Petroff D., Schöbel K., 2004, *MNRAS*, 355, 682
 Bardeen J. M., 1971, *ApJ*, 167, 425
 Bardeen J. M., Horowitz G. T., 1999, *Phys. Rev. D*, 60, 104030
 Dyson F. W., 1892, *Phil. Trans. R. Soc. A*, 184, 43
 Dyson F. W., 1893, *Phil. Trans. R. Soc. A*, 184, 1041
 Eriguchi Y., Sugimoto D., 1981, *Prog. Theor. Phys.*, 65, 1870
 Hachisu I., 1986, *ApJS*, 61, 479
 Kowalewsky S., 1885, *Astron. Nachr.*, 111, 37
 Meinel R., 2002, *Ann. Phys., Lpz.*, 11, 509
 Meinel R., 2004, *Ann. Phys., Lpz.*, 13, 600
 Meinel R., 2005, preprint (gr-qc/0506130)
 Neugebauer G., Meinel R., 1995, *Phys. Rev. Lett.*, 75, 3046
 Nozawa T., Stergioulas N., Gourgoulhon E., Eriguchi Y., 1998, *A&AS*, 132, 431
 Oppenheimer J., Volkov G., 1939, *Phys. Rev.*, 55, 374
 Poincaré H., 1885a, *C. R. Acad. Sci.*, 100, 346
 Poincaré H., 1885b, *Bull. Astron.*, 2, 109
 Poincaré H., 1885c, *Bull. Astron.*, 2, 405
 Schöbel K., Ansorg M., 2003, *A&A*, 405, 405
 Tooper R., 1965, *ApJ*, 142, 1541
 Wong C. Y., 1974, *ApJ*, 190, 675

This paper has been typeset from a $\text{\TeX}/\text{\LaTeX}$ file prepared by the author.